Journal of Alloys and Compounds 892 (2021) 162207

Contents lists available at ScienceDirect

Journal of Alloys and Compounds

journal homepage: www.elsevier.com/locate/jalcom

High microwave absorption performance in Nd-substituted BaM/GO through sol-gel and high energy ball milling process

Jinjie Liu[a,b,c], Xiaohua Feng[b,c,*], Shuangjie Wu[b,c], Ping Zhou[b,c], Jing Huang[b,c], Hua Li[b,c,*], Tongxiang Liang[a,**]

[a] School of Materials Science and Engineering, Jiangxi University of Science and Technology, Jiangxi 341000, China
[b] Key Laboratory of Marine Materials and Related Technologies, Zhejiang Key Laboratory of Marine Materials and Protective Technologies, Ningbo Institute of Materials Technology and Engineering, Chinese Academy of Sciences, Ningbo 315201, China
[c] Zhejiang Engineering Research Center for Biomedical Materials, Cixi Institute of BioMedical Engineering, Ningbo Institute of Materials Technology and Engineering, Chinese Academy of Sciences, Cixi 315300, China

ARTICLE INFO

Article history:
Received 6 July 2021
Received in revised form 7 September 2021
Accepted 29 September 2021
Available online 2 October 2021

Keywords:
Barium ferrite
Graphene oxide
Neodymium
Microwave absorption
Electromagnetic properties

ABSTRACT

In this paper, a series of compound materials with different proportions of rare earth neodymium (Nd) doped M-type barium ferrite (BaM) and the mixture Nd-BaM with graphene oxide (GO) are prepared through the sol-gel method and high-energy ball milling route. The surface morphology, composition and electromagnetic properties of those materials are analyzed through XRD, SEM, TG, Raman and the vector network analyzer. It is found that the Nd-BaM particle is adhered on the surface of GO with the nanometer size. The electromagnetic performance can be severely affected by the doping amounts of Nd and the blending amounts of GO. Moreover, the microwave absorption performance of the compounds is studied in the frequency range of 2–18 GHz. For $Nd_{0.15}$-BaM/3%GO, the minimum reflection loss is − 82.07 dB at 12.65 GHz and the scope of the effective absorption band is 6.08 GHz with a thickness of 2 mm. Because of its good impedance matching, the interface polarization and electron polarization between Nd-BaM and GO, the electromagnetic wave occurs multiple reflection in this material. Compared with pure BaM or BaM/GO, the Nd substituted BaM/GO has excellent microwave absorption performance, which has a certain prospect in the microwave absorbing field.

1. Introduction

Nowadays, with the development of science, technology and communication equipment, electromagnetic waves permeate our lives. For example, wireless network, TV and radio can produce electromagnetic waves, and electromagnetic waves have become the fourth largest source of pollution in the world [1,2]. Excessive electromagnetic waves can damage human health [3], the environment in which we live and the electrical equipment which we use [4]. Therefore, high-performance microwave absorbing material has been emerging [5,6].

Among them, M-type barium ferrite (BaM) shows strong capability of microwave absorption [7], because of its high magnetocrystalline anisotropy field and large magnetic loss [8], stemmed from its hexagonal magnetoplumbite structures with a hard magnetic property. The common synthetic routes of BaM are sol-gel [9,10], co-precipitation [11], solid phase reaction [12,13] and microemulsion [14,15] etc. Compared with other hexagonal ferrites, BaM has a wider effective absorption band. However, it is of high density [16], poor oxidation resistance and poor thermal stability. It can cause agglomeration due to dipole interaction between particles, which has negative effects on its magnetic loss [17]. These drawbacks strongly limit the application of BaM [18].

In order to improve the electromagnetic wave absorption performance of BaM, ion doping and material mixture are the common means to elevate the properties.

From the Table 1, many metal ions are selected to dope into BaM in order to improve the absorbing performance. The doping of ions can improve the absorbing properties of the material on the reflection loss and effective absorption band. Even if the same ion is

* Correspondence to: Ningbo Institute of Materials Technology and Engineering, Chinese Academy of Sciences. All rights reserved.1219 Zhongguan West Road, Ningbo, China (315201)
** Correspondence to: School of Materials Science and Engineering, Jiangxi University of Science and Technology, Jiangxi, 341000, People's Republic of China
E-mail addresses: xhfeng@nimte.ac.cn (X. Feng), lihua@nimte.ac.cn (H. Li), txliang@jxust.edu.cn (T. Liang).

https://doi.org/10.1016/j.jallcom.2021.162207
0925-8388/© 2021 Published by Elsevier B.V.

Table 1
Summarizes the microwave absorption performance of BaM doped with different ions.

Material	Method	RL_{min}/dB	The frequency of RL_{min}/GHz	EAB/GHz	d/mm	Ref.
Ni, Zr-BaM	Solid-state reaction	-60.6	About 15.9	7.68	2.1	[19]
Co-BaM	Co-precipitation	-16	17.0	/	1.5	[20]
BaM		Less than − 10	/		/	
Mn, Co, Ti-BaM	Solid-state reaction	-40.2	14.9	7.0	2.3	[21]
BaM		-27.4	12.34	0.14	3.9	
Mn, Ti, Co, Ni-BaM	Sol-gel	-52.8	13.4	5.8 (< − 15 dB)	1.8	[22]
Cu, Mg, Zr-BaM	Co-precipitation	-14.4	9.2	4	3.3	[23]
BaM		Less than − 10	/	/	/	
Al-BaM	Self-propagating combustion	-34.76	14.57	/	/	[24]
Cr-BaM		-27	13.26			
BaM		-25	/			
Mn, Cu, Ti-BaM	Conventional ceramic technique	-51.78	18.78	2.79 (< − 20 dB)	1.8	[25]
BaM		-5.7	17.75	/	1.8	
Eu-BaM	Sol-gel	-43	15.6	/	2	[26]
BaM		-16	8.8	/	2	
La-BaM	Electrospinning Heat treatment	-23.03	2	12.6	2	[27]
BaM		Less than − 10	/	/	/	
Cu, Ti-BaM	Sol-gel	-37	16.7	2.5	1.6	[28]
BaM		Less than − 10	/	/	/	
Co-BaM	Solid-state reaction	-32.1	11.2	5	2	[29]
BaM		-10.3	About 11	/	1.5	

doped, under different preparation conditions, the particle size, dispersibility and purity of barium ferrite are various, which leads to different reflection loss properties. Normally, rare earth metals is of good electromagnetic properties. Replacing some Fe^{3+} ions in BaM with rare earth ions of larger ionic radius will cause lattice distortion, which may improve the dielectric properties of BaM [30]. It is also found that the partly replacement can prohibit the growth, reduce the size and direction coercive force of crystal grains, which may be beneficial to the electromagnetic properties of BaM [31]. So we select Nd as the dopant, because Nd atom has a special electromagnetic structure and many unpaired electrons. These unpaired electrons can generate magnetic moments when they move on the orbit, which may greatly increases the magnetism of BaM [32].

BaM with carbon materials is an alternative way to improve the microwave absorption performance. Generally, nano carbon materials have excellent properties, such as excellent dielectric properties, high specific surface area, low density and high mechanical strength, which have certain benefits to the improvement of wave absorbing performance. A single magnetic material or a single dielectric material cannot meet the impedance matching, so it is necessary to combine nano carbon materials. Reduced graphene oxide (rGO) is a commonly used compounding agent in different proportions through different compounding approaches. It's reported when the content of rGO is 6%, the reflection loss of the sample reaches − 52.21 dB at 10.72 GHz, and the effective absorption band is 2.92 GHz through sol-gel method. With the addition of rGO, the saturation magnetization of BaM decreases and the polarization of the interface increases [33,34]. Beside rGO, the addition of other oxides such as Fe_3O_4 can effectively increases the heterogeneous interface, which is beneficial to the enhancement of interface polarization. The minimum reflection loss of rGO/BaM/Fe_3O_4 reaches − 46.04 dB at 15.6 GHz with a thickness of 1.8 mm [35]. Also, special microstructure may improve the dielectric properties and enhance the interface polarization of the BaM. It's reported that the nano expanded graphite (EG), carbon nanotube (CNT) and BaM compound form a sandwich three-dimensional network microstructure through the sol-gel method and self-growing route, the minimum reflection loss of CNT/EG/BaM reaches − 45.8 dB at 14.1 GHz with a thickness of 1.0 mm [36].

In this study, graphene oxide (GO) is selected as an additive to BaM. GO is a derivative of graphene-based materials, the oxidation process makes GO chemically stable. rGO is reduced on the basis of GO with the loss of oxidizing functional groups. There are lots of oxygen functional groups on the surface and edges of GO, such as hydroxyl, epoxide, carboxyl and other functional groups. These functional groups can be used as polarization centers to attenuate electromagnetic waves [37]. Also, GO has similar surface properties and layered structure to multilayer graphene [38]. By using the special structure of GO and the combination of ferrite materials, we get the synergistic reinforced composite material, which may improve the impedance matching of graphene materials. Certainly, the use of sheet GO can alleviate the agglomeration of BaM particles.

In view of the advantages of rare earth elements and nano-carbon materials, this research uses sol-gel method to replace Fe^{3+} with rare earth Nd^{3+}, which may change the magnetocrystalline anisotropy field of ferrite and increase the electromagnetic loss of the material in the magnetic field. After replacing Fe^{3+} with Nd^{3+} of larger ion radius, the lattice constant of the material may increase and the dielectric loss may increase [39,40]. Then, mixing Nd-BaM with GO through ball milling, the dielectric loss may increase again. The Nd-BaM/GO also have a certain complex permittivity and permeability, which promotes impedance matching, so that the electromagnetic wave in the material may effectively attenuate. Therefore, the purpose of this paper is to study the effect of Nd doping on the microwave absorption performance and the optimal ratio between GO and Nd-BaM for the application of electromagnetic wave absorption materials.

2. Materials and methods

2.1. Original materials

GO (purity: 95%) is purchased from Nanjing XFNANO Materials Tech Co. Ltd, China. Ferric nitrate ($Fe(NO_3)_3{\cdot}9H_2O$, purity: 98.5%), neodymium nitrate ($Nd(NO_3)_3$, purity: 99.9%), barium nitrate ($Ba(NO_3)_2$, purity: 99%), citric acid (purity: 99.5%) and ammonium hydroxide ($NH_3{\cdot}H_2O$, concentration: 25–28%) are all purchased from Sinopharm Chemical Reagent.

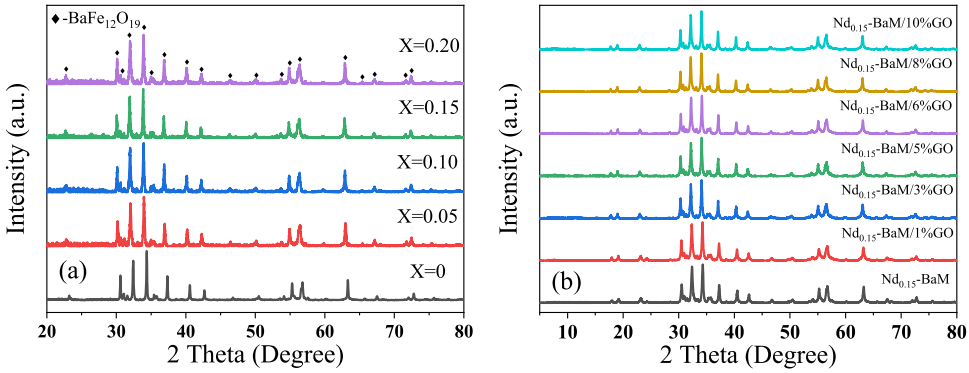

Fig. 1. XRD powder pattern of (a) Nd_x-BaM (x = 0, 0.05, 0.1, 0.15, 0.2) and (b) $Nd_{0.15}$-BaM/GO.

2.2. Synthesis of materials

Preparation process of Nd doped BaM: $Fe(NO_3)_3{\cdot}9H_2O$, $Nd(NO_3)_3$, $Ba(NO_3)_2$ and citric acid are taken as precursor. The proportional Fe $(NO_3)_3{\cdot}9H_2O$, $Nd(NO_3)_3$ and $Ba(NO_3)_2$ are dissolved in a small amount of deionized water and the molar ratio between them is (12-x): x: 1, x is equal to 0, 0.05, 0.1, 0.15, 0.2. Citric acid and metal ions (molar ratio is 1:1) are added to the solution, into which ammonium hydroxide is slowly added to adjust pH to 7.0. Then, the solution is heated in a water bath at 80 ℃ and kept for 6 h with continuous vigorous stirring. The obtained gel is moved to the muffle furnace, heated from room temperature to 200 ℃ at a heating rate of 2 ℃/min for 2 h, then the obtained powder is crushed in a mortar. The powder is heated again in a muffle furnace, from room temperature to 850 ℃ with a rate of 5 ℃/min for 3 h. The final powder with different value of x are named as BaM, $Nd_{0.05}$-BaM, $Nd_{0.1}$-BaM, $Nd_{0.15}$-BaM, $Nd_{0.20}$-BaM.

GO is mixed into the BaM or Nd-BaM according to 1%, 3%, 5%, 6%, 8%, 10% of the mass ratio (the mass ratio = GO/ BaM, or GO/Nd-BaM). The mixture is milled through ball milling equipment with an iron ball and an agate tank. The mass ratio of ball to powder is 10:1. The rotational speed of ball grinding is 300 rpm/min for 4 h. The resulting powder is the complex compound Nd-BaM/GO with different mass ratio.

2.3. Characterizations

The structure and phase of samples are identified from X-ray diffraction (XRD, D8 Advance Davinci, Germany, 40 kV and 40 mA of Cu Kα) at the scattering angle of 20° ≤ 2θ ≤ 80°. The morphologies of samples are observed by scanning electron microscopy (SEM, Zeiss Gemini 300, Germany). The thermal stabilities of the samples are characterized in air atmosphere with a heating rate of 10 ℃/min and a heating range of 50–800 ℃ (TG , STA 449F3, Germany). Raman spectra are recorded on a Raman spectrometer (Renishaw inVia Reflex, Britain) with Al Kα radiation. The temperature ranges from 50 ℃ to 800 ℃. The vector network analyzer (VNA, Agilent N5225A) is used to measure the complex permittivity and permeability of compound material in the frequency range of 2–18 GHz with a demanded shape sample.

3. Results and discussion

The phase of the samples is determined by XRD, and the typical diffraction pattern are as follows. All the peaks of the samples correspond to BaM peaks (Fig. 1).

The peaks at 30.83°, 32.20°, 34.11°, 37.08°, 40.32°, 42.42°, 55.06°, 56.33°, 56.60° and 63.06° of all samples in the XRD patterns are related to the (008), (107), (114), (203), (205), (206), (217), (304), (2011) and (1015) diffractions of BaM. After Nd doping, the XRD peaks of all samples slightly shift to the left. According to Braggs law:

$$2d \sin\theta = n\lambda \tag{1}$$

where d is the distance between parallel atomic planes, λ is the wavelength of the incident wave, θ is the angle between the incident light and the crystal plane and n is the number of reflection orders. The left shift of the diffraction peak means that the angle becomes smaller, that means crystalline interfacial spacing becomes larger (Fig. 1.a). In this paper, part of the Nd^{3+} replace the position of Fe^{3+}, the ionic radius of Nd^{3+} is larger than Fe^{3+}, so the unit cell parameter becomes larger, and the d value also becomes larger. The test results are consistent with the Braggs theory. The addition of GO has little effect on the characteristic diffraction peaks of Nd doped BaM, which indicates that no chemical reaction occurred between Nd doped BaM and GO (Fig. 1.b). The characteristic diffraction peak of GO is around 10.5°, since the diffraction peak intensity of Nd doped BaM masks the diffraction peak of GO, so it is difficult to see the diffraction peak of GO from Fig. 1b at this angle.

The grain size of Nd doped BaM is calculated by the XRD soft. It indicated that the more Nd element is doped, the smaller the grain size of the powder is obtained (Table 2), that means the addition of rare earth can inhibit the growth of grains.

SEM morphology of the Nd-BaM/GO compound shows that as the proportion of GO is gradually increases, the GO flakes is also increasing (Fig. 2.a, b). BaM particles are attached to the GO sheet and the distribution is relatively even (Fig. 2.c). The particles are all nanoscale, ranging from 50 to 200 nm, with spherical and irregular shapes and some of them appear the state of agglomeration. Particle sintering temperature and magnetic properties are the main factors affecting agglomeration, usually it's positively correlated. From the element distribution mapping (Fig. 2.c-Fe, Ba, C, O), the BaM particles do adhere to the GO sheet. The content of rare earth Nd is too low to be detected.

Table 2
The grain size of Nd doped BaM with different molar ratio.

Composition/x	Grain size/nm
0	89.1
0.05	79.1
0.1	77.3
0.15	62.3
0.2	48.8

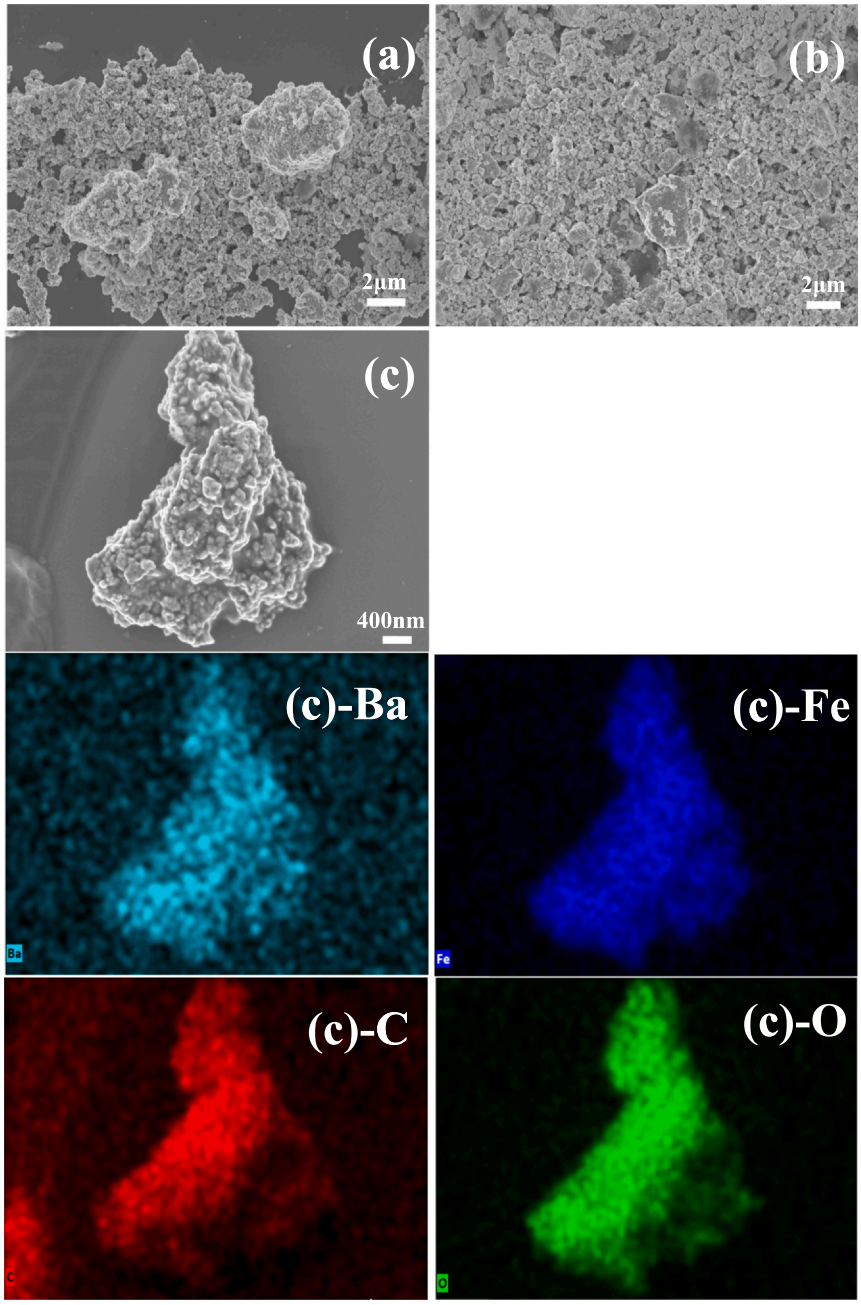

Fig. 2. SEM image of (a) $Nd_{0.15}$-BaM/1%GO, (b) $Nd_{0.15}$-BaM/10%GO, (c) EDS of $Nd_{0.15}$-BaM/3%GO.

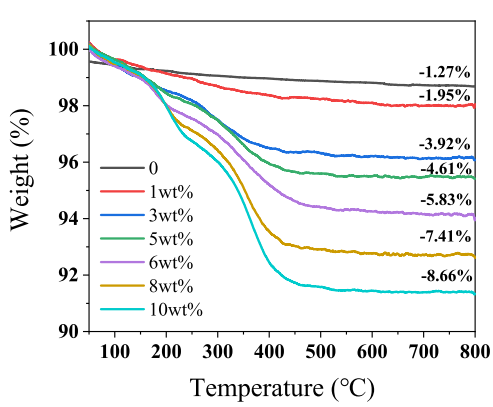

Fig. 3. TG curves of $Nd_{0.15}$-BaM and $Nd_{0.15}$-BaM/GO under air atmosphere.

The real GO blending amount can be obtained by TG test. It clearly shows that the mass of the decomposed samples is different under the increasing temperature (Fig. 3). When the temperature is less than 100 ℃, the water molecules in the compound will evaporate and cause a slight loss of mass [41]. When the temperature is between 200 °C and 400 °C, GO begins to be thermally decomposed until around 500 °C, the curve tends to be flat, and GO is completely decomposed, so that the content of GO in the sample can be analyzed. There is 1.27% loss item in the original $Nd_{0.15}$-BaM material. That means the material is easy to absorb moisture. The mixing ratio of GO will also be affected by the moisture absorption of the original material, especially when the GO content is low. It can be seen from Fig. 3 that the true content of GO is slightly lower than the amount when it is added, since there will be a small amount of GO loss during the ball milling process.

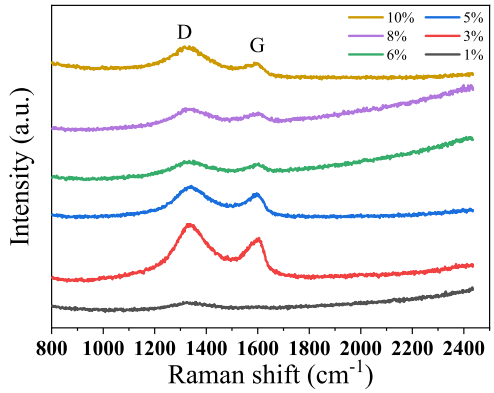

Fig. 4. Raman spectra of $Nd_{0.15}$-BaM/1, 3, 5, 6, 8, 10%GO.

In order to further prove the existence of GO, the samples are analyzed by Raman spectroscopy (Fig. 4). The D peak of the samples is located at 1329 cm^{-1}, and the D-peak is related to the lattice defect of carbon atoms. G peak is located at 1600 cm^{-1}, which is related to the in-plane stretching vibration of the sp^2 hybridization of carbon atoms [42], and proved the presence of GO in the samples. The D peak intensity of the sample with 3% GO is obviously higher than that of other samples, indicating that multiple defects are generated and the dipolar polarization is strengthened.

The dielectric properties and magnetic properties of absorbing electromagnetic wave materials are determined by the complex permittivity ($\varepsilon_r = \varepsilon' - j\varepsilon''$) and complex permeability ($\mu_r = \mu' - j\mu''$) of the materials. The real part of the complex permittivity and the complex permeability represents the electromagnetic storage capacity, and the imaginary part represents the electromagnetic consumption capacity[43]. The change of ε' is not regular with the influence of doping amount. The ε' of $Nd_{0.1}$-BaM is the largest, the curve is relatively flat at low frequency and has obvious fluctuation at high frequency (Fig. 5.a). In terms of the relationship between the ε'' and frequency, the amount of doping has no obvious effect on the value of ε'' except $Nd_{0.15}$-BaM has two sharp resonant peaks at 11.3 GHz and 12.7 GHz, so the electromagnetic waves consumption is more serious at these two frequencies (Fig. 5.b). The ε'' of $Nd_{0.05}$-BaM and $Nd_{0.2}$-BaM has a little different at about 13.3 GHz. $Nd_{0.05}$-BaM has two obvious characteristic peaks, which will be caused by depolarization or interface polarization. The values ε'' of $Nd_{0.2}$-BaM are almost less than 0.2. That means the electromagnetic consumption capacity of $Nd_{0.2}$-BaM is weaker than that of $Nd_{0.05}$-BaM at this frequency range.

The μ' value is decreased with the increase of frequency. The imaginary permeability is also fluctuated slightly with frequency. Both $Nd_{0.15}$-BaM and $Nd_{0.2}$-BaM have obvious resonance peaks at 10–15 GHz. These trends indicate that the addition of Nd increases the magnetic loss of the compounds (Fig. 5.c, d).

When the GO content is 6%, 8% and 10%, the electromagnetic properties have little change (Fig. 6). Only $Nd_{0.15}$-BaM/3%GO has both dielectric loss and magnetic loss, so it of a better microwave

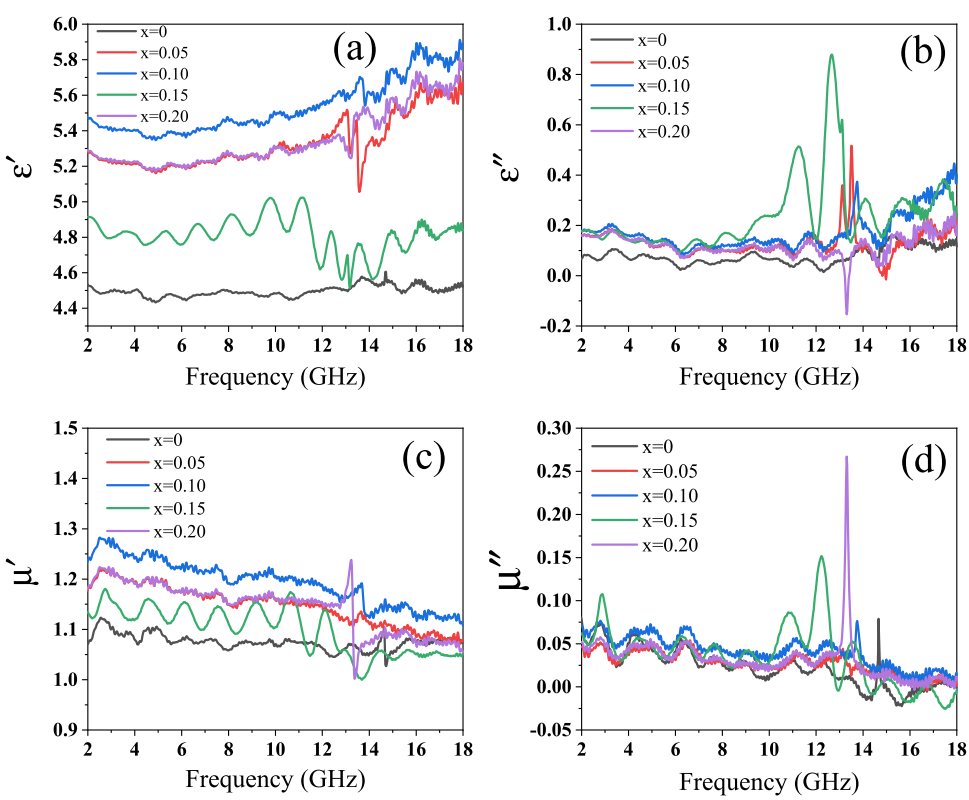

Fig. 5. (a) The real permittivity (ε'), (b) imaginary permittivity (ε''), (c) real permeability (μ') and (d) imaginary permeability (μ'') of the Nd_x-BaM.

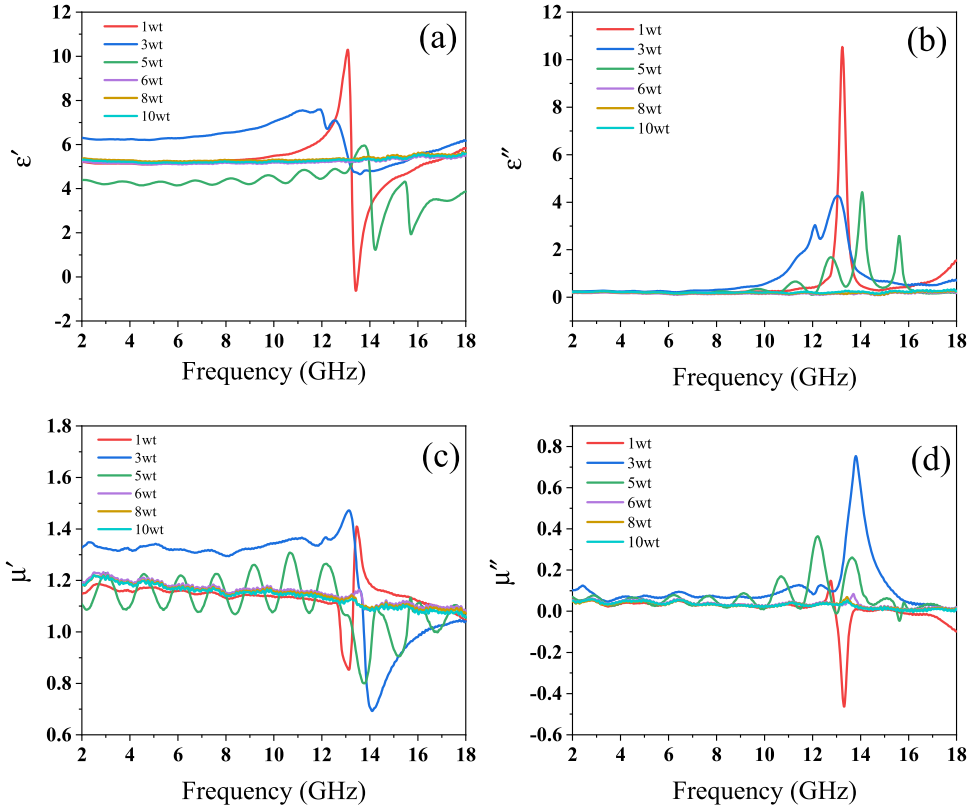

Fig. 6. (a) The real permittivity (ε'), (b) imaginary permittivity (ε''), (c) real permeability (μ') and (d) imaginary permeability (μ'') of the $Nd_{0.15}$-BaM/GO.

absorbing performance. The detailed explanation of this phenomenon is presented in the following test results.

The energy loss of electromagnetic waves causes the reflection loss. The reflection loss usually describes the absorbing performance of materials. According to the transmission line theory, *RL* can be calculated by the formulas as follows [44]:

$$RL = 20\log_{10}\left|\frac{Z_{in} - Z_0}{Z_{in} + Z_0}\right| \tag{2}$$

$$Z_{in} = Z_0\sqrt{\frac{\mu_r}{\varepsilon_r}}\tanh\left(j\left(\frac{2\pi fd}{c}\right)\sqrt{\mu_r\varepsilon_r}\right) \tag{3}$$

where Z_{in} represents the normalized input impedance of the absorber, Z_0 is the impedance of free space, μ_r is the complex permeability of the material, ε_r is the complex permittivity, f is the frequency of electromagnetic waves, d is the thickness of the absorber, and c is the speed of light.

Under different amounts of the Nd doping, *RL* changes with frequency and thickness. The performance of the samples has been slightly improved after Nd doping. At 2.0 mm and 2.5 mm, the *RL* value of the Nd-BaM is not ideal, which is caused by weak dielectric loss and impedance mismatch. After the mixing of pure BaM and GO by ball milling process, the absorbing performance of the sample is not improved significantly with the amount of GO, because the amount of GO is too small and does not have much influence on the dielectric properties of the compound material (Fig. 7.c, d). However, after mixing the same amount of GO with Nd-BaM through ball milling, we find that its microwave absorbing performance has been significantly improved (Fig. 7.e, f). At 2.0 mm, the absorption performance of $Nd_{0.15}$-BaM/3%GO is the best, the reflection loss reaches −82.07 dB at 12.65 GHz, and the effective absorption broadband (RL < −10 dB) is 6.08 GHz, and at 2.5 mm, the microwave absorbing performance of the material is similar to the performance when the thickness is 2 mm. In order to make the material meet the requirements of light weight, the thickness of the material should be as thin as better. Nd element doped and GO additive are of a synergistic effect in the BaM material, which improve the microwave absorbing performance obviously.

In order to further examine the absorbing performance of $Nd_{0.15}$-BaM/3%GO, the various absorbing performance indicators is evaluated at different thickness, frequency. The total effective absorption band is 6.67 GHz (9.99–16.66 GHz), and the minimum *RL* at 2.0 mm is −82.07 dB, and the minimum *RL* is −53.51 dB, which is much better than the performance of materials that GO compounds with other contents (Fig. 8.a). The higher ε' and ε'' appear at 11–13 GHz. ε'' has two obvious relaxation peaks at 12.11 GHz and 13.05 GHz, which is caused by dipole polarization or interface polarization. The imaginary part and real part of its permeability remain basically unchanged at 2–18 GHz, with a tiny change around 14 GHz. The

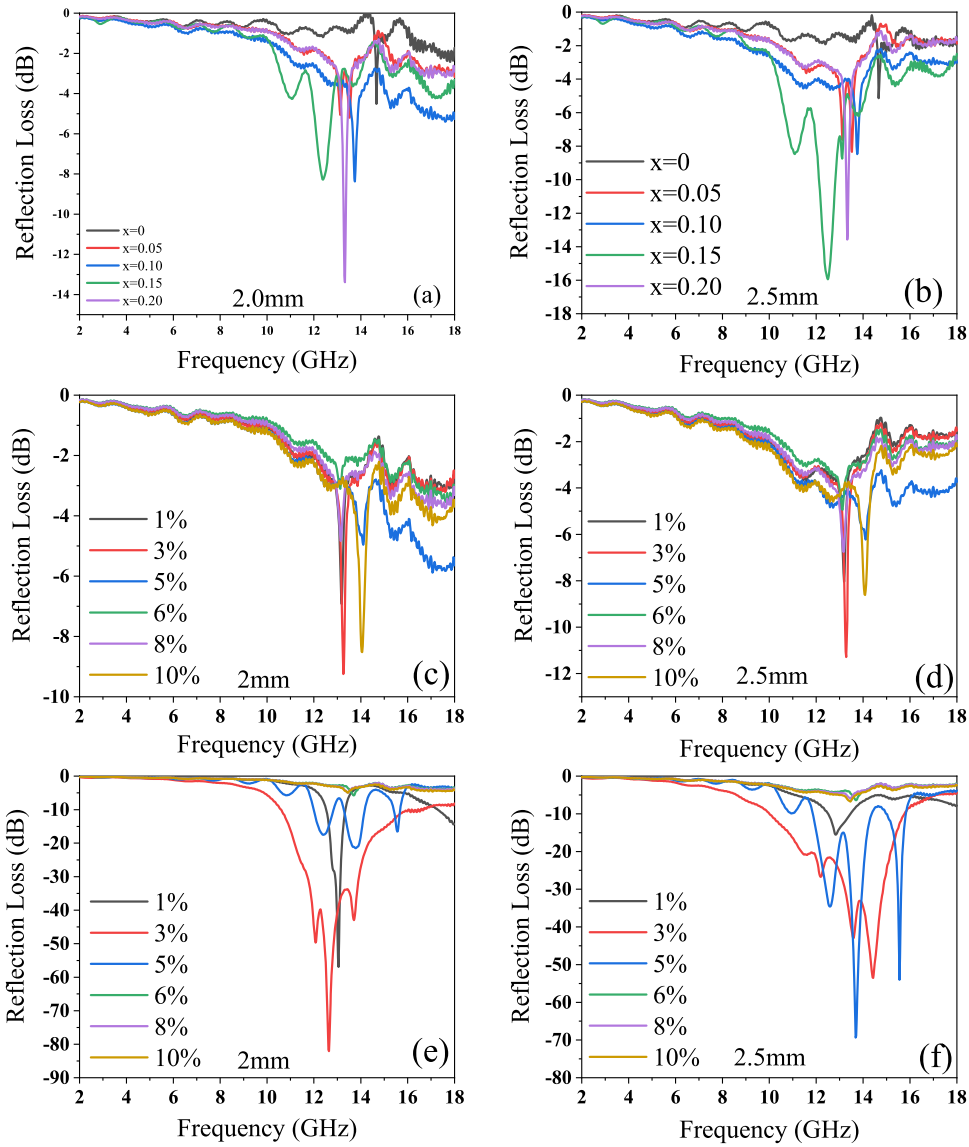

Fig. 7. Reflection loss of (a-b) $BaNd_xFe_{12-x}O_{19}$, (c–d) BaM/GO, (e-f) $Nd_{0.15}$-BaM/GO with the absorber thickness of 2 mm and 2.5 mm.

decrease of μ' and the increase of μ'' directly lead to the increase of $tan\,\delta\mu$, which is caused by domain wall resonance. Compared with ε' and ε'', the μ' and μ'' values of this sample are relatively low at 1.3 and 0.1 (Fig. 8.b). The difference between the dielectric loss tangent ($tan\,\delta\varepsilon$) and the magnetic loss tangent ($tan\,\delta\mu$) of this compound material is small, and the similarity of $tan\,\delta\varepsilon$ and $tan\,\delta\mu$ is conducive to the impedance matching of the material [45]. The highest values of $tan\,\delta\varepsilon$ and $tan\,\delta\mu$ are 0.81 and 0.91, respectively, which proves that this material is an electromagnetic microwave absorbing material that cooperates with dielectric loss and magnetic loss, so it has the highest electromagnetic microwave absorption performance [46] (Fig. 8.c). Compared with similar materials reported in the literature (Table 3), especially their electromagnetic wave absorption properties. We can observe that $Nd_{0.15}$-BaM/3%GO has a lowest *RL* value. Compared with the same thickness of material, its effective absorption band is wider, which also shows that $Nd_{0.15}$-BaM/3%GO has a broad application background in lightweight electromagnetic wave absorption coatings.

In summary, the excellent electromagnetic wave absorption performance of $Nd_{0.15}$-BaM/3%GO can be explained from the following aspects: (i) The nanocomposite has outstanding impedance matching, that means the incident electromagnetic wave can enter the interior of the compound well; (ii) This material can form more interfaces, which provides rich interfacial polarization for the reflection of electromagnetic waves; (iii) The material obtained is composed of GO and Nd-BaM particles, which will cause dielectric

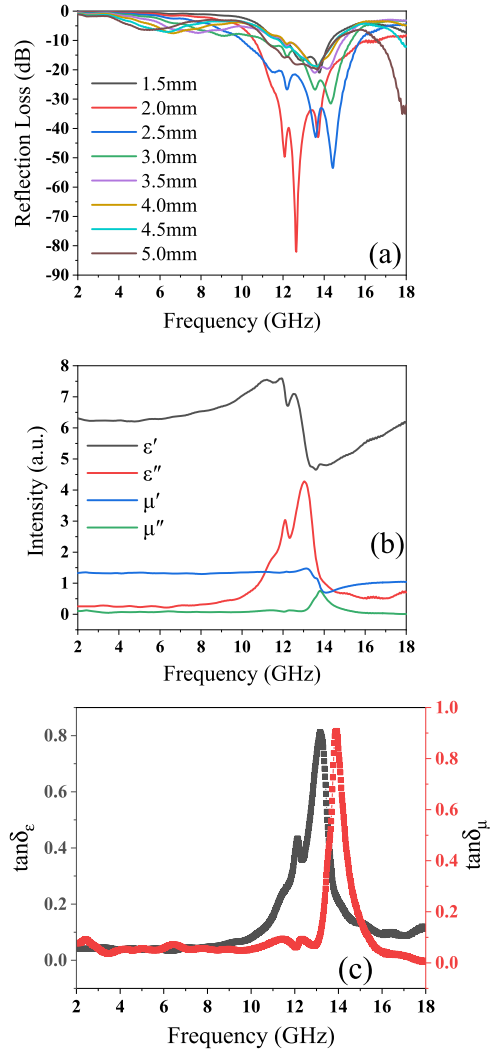

Fig. 8. (a) Reflection loss, (b) ε', ε'', μ', μ'', (c) tan δ_ε and tan δ_μ of the $Nd_{0.15}$-BaM/3%GO.

Table 3
Microwave absorption performance of various similar materials.

Samples	RL_{min}/dB	Thickness/ mm	EAB/GHz	Ref.
Co-BaM	-32.1 (11.2 GHz)	2.0	5.0 (8.5–13.5)	[29]
Cr-BaM	-41 (12.0 GHz)	2.55	——	[47]
RGO/BaM	-52.21 (10.72 GHz)	2.1	2.92	[33]
graphite/BaM	-30.0 (9.2 GHz)	3.0	0.6	[48]
BaM@C	-73.42 (17.84 GHz)	1.4	——	[49]
$Nd_{0.15}$-BaM/3%GO	-82.07 (12.65 GHz)	2.0	6.67 (9.99–16.67)	This work

loss and magnetic loss at the same time. The double loss mechanism is the key factor to improve the absorbing performance; (iv) The defects and functional groups in GO can produce dipole polarization, it may contribute to the electromagnetic attenuation.

4. Conclusion

In summary, the compound materials of Nd-doped BaM with GO additive can be successfully prepared through two simple processes of sol-gel method and high-energy ball milling. The structure and morphology of the synthesized compounds are characterized by XRD, SEM, Raman, and TG. It can be clearly seen on the SEM that the magnetic Nd-BaM particles are attached to the surface of GO. Through the inspection of its dielectric loss and magnetic loss properties, it demonstrates excellent microwave absorption performance. The minimum reflection loss of $Nd_{0.15}$-BaM/3%GO at 12.65 GHz is −82.07 dB and the effective bandwidth is 6.08 GHz when the coating thickness is 2.0 mm, which has the best performance compared with similar materials reported in the current literature. With the apparent absorption loss and good impedance matching, this kind of nanocomposite can expand its application market.

CRediT authorship contribution statement

Jinjie Liu: Investigation, Formal analysis, Writing – original draft. **Xiaohua Feng:** Conceptualization, Project administration, Writing – review & editing. **Shuangjie Wu:** Partial data test. **Ping Zhou:** Data curation. **Jing Huang:** Partial data test. **Hua Li:** Verification. **Tongxiang Liang:** Supervision.

Declaration of Competing Interest

The authors declare that they have no known competing financial interests or personal relationships that could have appeared to influence the work reported in this paper.

Acknowledgements

This work is supported by Chinese Academy of Sciences Key Project (ZDRW-CN-2019-3), the National Natural Science Foundation of China through Grant no. 51802322, the S&T Innovation 2025 Major Special Programme of Ningbo (2018B10054), and K.C. Wong Education Foundation (Grant # GJTD-2019-13).

References

[1] Y.T. Zhang, C.L. Liu, K.S. Peng, Y.F. Cao, G. Fang, Y.J. Zhang, Synthesis of broad microwave absorption bandwidth Zr^{4+}-Ni^{2+} ions gradient-substituted barium ferrite, J. Ceram. Int. 46 (2020) 25808–25816.
[2] D.F. Zhou, H. Yuan, Y.L. Xiong, G.Q. Luo, Q. Shen, Constructing highly directional multilayer cell structure (HDMCS) towards broadband electromagnetic absorbing performance for CNTs/PMMA nanocomposites foam, J. Compos. Sci. Technol. 203 (2021) 108614–108623.
[3] J.Z. He, X.X. Wang, Y.L. Zhang, M.S. Cao, Small magnetic nanoparticles decorating reduced graphene oxides to tune the electromagnetic attenuation capacity, J. Mater. Chem. C 4 (29) (2016) 7130–7140.
[4] N.Y. Chen, J.T. Zhou, Z.J. Yao, Y.M. Lei, R.Y. Tan, Y.X. Zuo, W.J. Zheng, Z.B. Jiao, Fabrication of Nd-doped Ni–Zn ferrite/multi-walled carbon nanotubes composites with effective microwave absorption properties, J. Ceram. Int. 47 (8) (2021) 10545–10554.
[5] Y. Li, S. Li, T. Zhang, L.L. Shi, S.T. Liu, Y. Zhao, 3D hierarchical Co_3O_4/reduced graphene oxide/melamine derived carbon foam as a comprehensive microwave absorbing material, J. Alloy. Compd. 792 (2019) 424–431.
[6] Y.X. Huang, H.Y. Zhang, G.X. Zeng, Z.H. Li, D.F. Zhang, H.P. Zhu, R.F. Xie, L.M. Zheng, J.H. Zhu, The microwave absorption properties of carbon-encapsulated nickel nanoparticles/silicone resin flexible absorbing material, J. Alloy. Compd. 682 (2016) 138–143.
[7] Z. Durmus, A. Durmus, H. Kavas, Synthesis and characterization of structural and magnetic properties of graphene/hard ferrite nanocomposites as microwave-absorbing material, J. Mater. Sci. 50 (3) (2014) 1201–1213.
[8] Y.D. Chang, Y. Zhang, L. Li, S.Q. Liu, Z. Liu, H. Chang, X. Wang, Microwave absorption in 0.1–18 GHz, magnetic and structural properties of $SrFe_{12-x}Ru_xO_{19}$ and $BaFe_{12-x}Ru_x$ O_{19}, J. Alloy. Compd. 818 (2020) 152930–152937.
[9] M. Verma, A.P. Singh, P. Sambyal, B.P. Singh, S.K. Dhawan, V. Choudhary, Barium ferrite decorated reduced graphene oxide nanocomposite for effective electromagnetic interference shielding, J. Phys. Chem. Chem. Phys. 17 (3) (2015) 1610–1618.
[10] H. Gong, S.J. Tan, J. Zheng, K.S. Peng, Y.T. Zhang, Y.J. Hu, S.J. Duan, G.Y. Xu, Enhanced microwave absorption properties of flake-shaped FeCo/$BaFe_{12}O_{19}$ composites, J. Ceram. Int. 47 (2021) 12389–12396.
[11] M. Khandani, M. Yousefi, S.S.S. Afghahi, M.M. Amini, M.B. Torbati, An investigation of structural and magnetic properties of Ce–Nd doped strontium hexaferrite nanoparticles as a microwave absorbent, J. Mater. Chem. Phys. 235 (2019) 121722–121730.
[12] W. Widanarto, M. Effendi, S.K. Ghoshal, C. Kurniawan, E. Handoko, M. Alaydrus, Bio-silica incorporated barium ferrite composites: evaluation of structure,

morphology, magnetic and microwave absorption traits, J. Curr. Appl. Phys. 20 (5) (2020) 638–642.
[13] D. Wang, A. Khesro, S. Murakami, A. Feteira, Q.L. Zhao, I. Reaney, Temperature dependent, large electromechanical strain in Nd-doped $BiFeO_3$-$BaTiO_3$ lead-free ceramics, J. Eur. Ceram. Soc. 37 (4) (2017) 1857–1860.
[14] A.A. Rodriguez-Rodriguez, M.B. Moreno-Trejo, M.J. Melendez-Zaragoza, V. Collins-Martinez, A. Lopez-Ortiz, E. Martinez-Guerra, M. Sanchez-Dominguez, Spinel-type ferrite nanoparticles: synthesis by the oil-in-water microemulsion reaction method and photocatalytic water-splitting evaluation, Int. J. Hydrog. Energy 44 (24) (2019) 12421–12429.
[15] K. Pemartin, C. Solans, J. Alvarez-Quintana, M. Sanchez-Dominguez, Synthesis of Mn–Zn ferrite nanoparticles by the oil-in-water microemulsion reaction method, J. Colloids Surf. A: Physicochem. Eng. Asp. 451 (2014) 161–171.
[16] L.X. Wang, Y.K. Guan, X. Qiu, H.L. Zhu, S.B. Pan, M.X. Yu, Q.T. Zhang, Efficient ferrite/Co/porous carbon microwave absorbing material based on ferrite@metal–organic framework, J. Chem. Eng. J. 326 (2017) 945–955.
[17] Z. Chen, D. Mu, T. Liu, Z. He, J. Ouyang, PANI/$BaFe_{12}O_{19}$@Halloysite ternary composites as novel microwave absorbent, J. Colloid Interface Sci. 582 (Pt A) (2021) 137–148.
[18] T. Zhao, X. Ji, W. Jin, S.S. Guo, H.Y. Zhao, W.H. Yang, X.Q. Wang, C.Y. Xiong, A.L. Dang, H. Li, T.H. Li, S.M. Shang, Z.F. Zhou, Electromagnetic wave absorbing properties of aligned amorphous carbon nanotube/$BaFe_{12}O_{19}$ nanorod composite, J. Alloy. Compd. 703 (2017) 424–430.
[19] K.Z. Shi, J. Li, S. He, H. Bai, Y. Hong, Y. Wu, D.C. Jia, Z.X. Zhou, A superior microwave absorption material: Ni^{2+}-Zr^{4+} co-doped barium ferrite ceramics with large reflection loss and broad bandwidth, J. Curr. Appl. Phys. 19 (7) (2019) 842–848.
[20] N. Tran, M.Y. Lee, B.W. Lee, Microwave absorption properties of cobalt-doped $BaFe_{12}O_{19}$ hexaferrites, J. Korean Phys. Soc. 77 (12) (2020) 1125–1134.
[21] H. Li, L. Zheng, D. Deng, X. Yi, M. Zhang, Multiple natural resonances broaden microwave absorption bandwidth of substituted M-type hexaferrites, J. Alloy. Compd. 862 (2021) 158638–158650.
[22] P.Y. Meng, K. Xiong, K. Ju, S.N. Li, G.L. Xu, Wideband and enhanced microwave absorption performance of doped barium ferrite, J. Magn. Magn. Mater. 385 (2015) 407–411.
[23] H. Nikmanesh, M. Moradi, G.H. Bordbar, R.S. Alam, Effect of multi dopant barium hexaferrite nanoparticles on the structural, magnetic, and X-Ku bands microwave absorption properties, J. Alloy. Compd. 708 (2017) 99–107.
[24] J.X. Qiu, M.Y. Gu, H.G. Shen, Microwave absorption properties of Al- and Cr-substituted M-type barium hexaferrite, J. Magn. Magn. Mater. 295 (3) (2005) 263–268.
[25] A. Ghasemi, A. Hossienpour, A. Morisako, A. Saatchi, M. Salehi, Electromagnetic properties and microwave absorbing characteristics of doped barium hexaferrite, J. Magn. Magn. Mater. 302 (2) (2006) 429–435.
[26] F. Khedemi, A. Poorbafrani, P. Kameli, H. Salamati, Structural, magnetic and microwave properties of eu-doped barium hexaferrite powders, J. Supercond. Nov. Magn. 25 (2) (2012) 525–531.
[27] C.J. Li, B. Wang, J.N. Wang, Magnetic and microwave absorbing properties of electrospun $Ba_{(1-x)}La_xFe_{12}O_{19}$ nanofibers, J. Magn. Magn. Mater. 324 (7) (2012) 1305–1311.
[28] S.N. Li, K. Xiong, P.Y. Meng, X.H. Ren, Sol-gel synthesis of copper(II) and titanium (IV) ions co-doped barium ferrite submicrometer crystals and their microwave absorption performance, J. Mater. Sci.-Mater. Electron. 26 (7) (2015) 5318–5325.
[29] G. Feng, W. Zhou, H.W. Deng, D. Chen, Y.C. Qing, C.H. Wang, F. Luo, D.M. Zhu, Z.B. Huang, Y.Y. Zhou, Co substituted $BaFe_{12}O_{19}$ ceramics with enhanced magnetic resonance behavior and microwave absorption properties in 2.6–18 GHz. J. Ceram. Int. 45 (11) (2019) 13859–13864.
[30] J. Zhao, J. Yu, Y. Xie, Z.G. Le, X.W. Hong, S.Q. Ci, J.H. Chen, X.Y. Qing, W.J. Xie, Z.H. Wen, Lanthanum and neodymium doped barium ferrite-TiO_2/MCNTs/poly (3-methyl thiophene) composites with nest structures: preparation, characterization and electromagnetic microwave absorption properties, J. Sci. Rep. 6 (2016) 20496.
[31] N. Yasmin, S. Yasmin, M. Zahis, S.F. Gillani, M.U. Islam, M. Altaf, H.M. Khan, M. Safdar, M. Mirza, Impact of Ho-Ni substitution on structural, morphological and dielectrical characteristics of $BaFe_{12}O_{19}$ M-type hexagonal ferrite, J. Phys. B: Condens. Matter 581 (2020) 411950.
[32] E. Ahilandeswari, R. Rahesh Kanna, K. Sakthipandi, Synthesis of neodymium-doped barium nanoferrite: analysis of structural, optical, morphological, and magnetic properties, J. Phys. B: Condens. Matter 599 (2020) 412425–412436.
[33] S. Goel, A. Garg, R. Gupta, A. Dubey, Development of RGO/$BaFe_{12}O_{19}$-based composite medium for improved microwave absorption applications, J. Appl. Phys. A 126 (6) (2020) 436–446.
[34] M. Verma, A.P. Singh, P. Sambyal, B.P. Singh, S.K. Dhawan, V. Choudhary, Barium ferrite decorated reduced graphene oxide nanocomposite for effective electromagnetic interference shielding, J. Phys. Chem. Chem. Phys. 17 (3) (2015) 1610–1618.
[35] S.Q. Jiao, M.Z. Wu, X.X. Yu, H.B. Hu, Z.M. Bai, P. Dai, T.T. Jiang, H. Bi, G. Li, RGO/$BaFe_{12}O_{19}$/Fe_3O_4 nanocomposite as microwave absorbent with lamellar structures and improved polarization interfaces, J. Mater. Res. Bull. 108 (2018) 89–95.
[36] T.K. Zhao, W.B. Jin, X.L. Ji, H.B. Yan, Y.T. Jiang, Y. Dong, Y.L. Yang, A.L. Dang, H. Li, T.H. Li, S.M. Shang, Z.F. Zhou, Synthesis of sandwich microstructured expanded graphite/barium ferrite connected with carbon nanotube composite and its electromagnetic wave absorbing properties, J. Alloy. Compd. 712 (2017) 59–68.
[37] X.X. Wang, B.Q. Zhang, W. Zhang, M.X. Yu, L. Cui, X.Y. Cao, J.Q. Liu, Super-light Cu@Ni nanowires/graphene oxide composites for significantly enhanced microwave absorption performance, J. Sci. Rep. 7 (1) (2017) 1584–1596.
[38] J. Yan, Y. Huang, S.H. Zhou, X.P. Han, P.B. Liu, Preparation and microwave absorption properties of nanomesh poly (3,4-ethylenedioxythiophene) covalently functionalized graphene oxide, J. Mater. Sci.: Mater. Electron. 30 (5) (2019) 5273–5283.
[39] J. Yang, W. Yang, F. Li, Y.C. Yang, Research and development of high-performance new microwave absorbers based on rare earth transition metal compounds: a review, J. Magn. Magn. Mater. 497 (2020) 165961–165971.
[40] A. Nikzad, R. Parcizi, Presence of neodymium and gadolinium in cobalt ferrite lattice: structural, magnetic and microwave features for electromagnetic wave absorbing, J. Rare Earth 38 (4) (2020) 411–417.
[41] X.Q. Xu, F.T. Ran, H. Lai, Z.J. Cheng, T. Lv, L. Shao, Y.Y. Liu, In situ confined bimetallic metal-organic framework derived nanostructure within 3D interconnected bamboo-like carbon nanotube networks for boosting electromagnetic wave absorbing performances, J. ACS Appl. Mater. Interfaces 11 (39) (2019) 35999–36009.
[42] Y.H. Cheng, M.Y. Tan, P. Hu, X.H. Zhang, B.Q. Sun, L.W. Yan, S.B. Zhou, Strong and thermostable SiC nanowires/graphene aerogel with enhanced hydrophobicity and electromagnetic wave absorption property, J. Appl. Surf. Sci. 448 (2018) 138–144.
[43] Q.T. Liu, X.F. Liu, H.B. Feng, H.C. Shui, R.H. Yu, Metal organic framework-derived Fe/carbon porous composite with low Fe content for lightweight and highly efficient electromagnetic wave absorber, J. Chem. Eng. J. 314 (2017) 320–327.
[44] S. Goel, A. Tyagi, A. Garg, S. Kumar, H.B. Baskey, R.K. Gupta, S. Tyagi, Microwave absorption study of composites based on CQD@$BaTiO_3$ core shell and $BaFe_{12}O_{19}$ nanoparticles, J. Alloy. Compd. 855 (2021) 157411–157420.
[45] Q. Liao, M. He, Y. Zhou, S.X. Nie, Y.J. Wang, S.C. Hu, H.Y. Yang, H.F. Li, Y. Tong, Highly cuboid-shaped heterobimetallic metal-organic frameworks derived from porous Co/ZnO/C microrods with improved electromagnetic wave absorption capabilities, J. ACS Appl. Mater. Interfaces 10 (34) (2018) 29136–29144.
[46] L. Wang, X. Yu, X. Li, J. Zhang, M. Wang, R.C. Che, MOF-derived yolk-shell Ni@C@ZnO Schottky contact structure for enhanced microwave absorption, Chem. Eng. J. 383 (2020) 123099–123108.
[47] H. Sozeri, F. Genc, M.A. Almessiere, I.S. Unver, A.D. Korkmaz, A. Baykal, Cr^{3+}-substituted Ba nanohexaferrites as high-quality microwave absorber in X band, J. Alloy. Compd. 779 (2019) 420–426.
[48] I. Ismail, I.R. Ibrahim, K.A. Matori, Z. Awang, M.M.M. Zulkimi, F.M. Idris, R. Nazlan, R.S. Azis, M.H.M. Zaid, S.N.A. Rusly, M. Ertugrul, Comparative study of single- and double-layer $BaFe_{12}O_{19}$-graphite nanocomposites for electromagnetic wave absorber applications, J. Mater. Res. Bull. 126 (2020) 110843–110852.
[49] Y.R. Liu, Y. Lin, H.B. Yang, Facile fabrication for core-shell $BaFe_{12}O_{19}$@C composites with excellent microwave absorption properties, J. Alloy. Compd. 805 (2019) 130–137.